

Dynamic Maximum Power Point Tracking of Photovoltaic Arrays Using Ripple Correlation Control

Trishan Eram, *Student Member, IEEE*, Jonathan W. Kimball, *Senior Member, IEEE*, Philip T. Krein, *Fellow, IEEE*, Patrick L. Chapman, *Senior Member, IEEE*, and Pallab Midya, *Senior Member, IEEE*

Abstract—A dynamically rapid method used for tracking the maximum power point of photovoltaic arrays, known as ripple correlation control, is presented and verified against experiment. The technique takes advantage of the signal ripple, which is automatically present in power converters. The ripple is interpreted as a perturbation from which a gradient ascent optimization can be realized. The technique converges asymptotically at maximum speed to the maximum power point without the benefit of any array parameters or measurements. The technique has simple circuit implementations.

Index Terms—Maximum power point tracking (MPPT), photovoltaic (PV), ripple correlation control (RCC).

I. INTRODUCTION

MANY MAXIMUM power point tracking (MPPT) techniques for photovoltaic (PV) systems are well established in the literature. The most commonly known are hill-climbing [1], fractional open-circuit voltage (V_{oc}) control [2], perturb and observe (P&O) [3], and incremental conductance (IncCond) [4]. There are lesser known, but sometimes very appropriate, methods such as maximizing load current or voltage [5], fractional short-circuit current (I_{sc}) control [6], array reconfiguration [7], linear current control [8], fuzzy control [9], neural network [10], dc link capacitor droop control [11], pilot cells [12], current sweep [13], limit-cycle control [14], and several others. Only one early example of each technique was given in the above list, even though we are aware of more than hundred and seventy papers on different MPPT techniques, dating from 1968. These techniques are reviewed and compared in [15]. Most of these techniques have been refined, adapted for digital signal processor (DSP) control, analyzed, etc. in many subsequent papers. The techniques vary in many aspects, including simplicity, speed of convergence, compensation for capacitance, digital versus analog implementation, sensors required, and need for parameterization.

Manuscript received May 11, 2005; revised November 29, 2005. This work was presented at the 27th Annual IEEE Power Electronics Specialists Conference (PESC'96). This work was supported by the National Science Foundation under Grant ECS-01-34208. Recommended by Associate Editor K. Ngo.

T. Eram, J. W. Kimball, P. L. Chapman, and P. T. Krein are with the University of Illinois at Urbana-Champaign, Urbana, IL 61801 USA (e-mail: esram@uiuc.edu).

P. Midya is with Freescale Semiconductor, Lake Zurich, IL 60047 USA.

Digital Object Identifier 10.1109/TPEL.2006.880242

Ripple correlation control (RCC) [16] yields fast and parameter-insensitive MPPT of PV systems. RCC has simple circuit implementations that are helpful to some users and is a general power electronics technique with several applications. In the context of PV arrays, we originally set forth RCC at a conference [17]. Since [17], more analysis and data have been generated to support the technique; these are presented here. RCC has the following general features relative to previous MPPTs:

- converges asymptotically to the maximum power point (MPP);
- uses array current and voltage ripple, which *must* already be present if a switching converter is used, to determine gradient information; no artificial perturbation is required;
- achieves convergence at a rate limited by switching period and the controller gain;
- does not rely on assumptions or characterization of the array or an individual cell;
- can compensate for array capacitive effects [18];
- has several straightforward circuit implementations, some of which are very inexpensive, analog versions;
- has a well developed theoretical basis [19].

These features taken together make RCC distinct from prior methods. Many factors must be considered when designing a photovoltaic converter, so that no single method can be claimed to be the best. Due to the inherent low cost of implementation, RCC would be well suited for a modular application, which would use many small converters rather than a few large, expensive converters. RCC is also appropriate for applications requiring a high rate of convergence, such as mobile systems that encounter rapidly changing light conditions (solar cars, for example).

A thorough comparison with all prior MPPT techniques is not within the scope of the paper. Instead, we compare RCC to similar techniques that attempt to drive the PV array power P to the MPP by driving gradients dP/dI or dP/dV to zero. RCC correlates [20] the time derivative of power with the time derivative of current or voltage. It has been shown [21] that this drives the power gradient to zero, though the explicit power gradient is not calculated. The derivatives are nonzero due to the natural ripple that occurs due to converter high switching frequency, thus the name “ripple correlation” control.

Reference [22] bears some similarity to RCC in that it looks at time derivatives of power and of duty ratio. A disturbance in duty ratio is used to generate a disturbance in power. The signs of the time derivatives are multiplied and integrated, much like

one version of RCC. However, RCC does not require intentional disturbance injection; instead, it uses the natural ripple already present in current and voltage (not duty ratio or frequency).

Since the original conference publication in 1996 [17], variations on RCC implementation have been derived [21], including a hysteresis-based version [21], [23], [24]. Several other related methods, since [17], have been introduced. In [25], simulated results show a linearization-based method for calculating dP/dV that can subsequently be driven to zero; using inherent power converter ripple is discussed but not shown. This seems to be the only other technique that suggests using inherent ripple. Others essentially average out the ripple and perturb the system at a lower frequency. In [26], a modified P&O method that is similar to a Newton–Raphson optimization is used. Only simulation results are shown, but the magnitude of the perturbation is reduced as the optimum is approached; this naturally occurs in RCC.

In [27], a slow dithering signal is used to disturb the power. The paper discusses a 90° phase shift in the current (or voltage) with respect to power at the MPP—exactly the same effect found in RCC. The difference in [27] is that the injection is an extra, low frequency signal, and not the naturally occurring power converter ripple. In [28] and [29], the authors present a method that disturbs duty cycle or frequency and observes power. However, the disturbance is again intentional and necessarily at a low frequency.

References [30] and [31] also use inherent ripple as a perturbation to perform MPPT. The inherent ripple comes from the fact that, in single-phase systems connected to the utility grid, instantaneous power oscillates at twice the line frequency. The perturbation is external and load-dependent, unlike the internal perturbation (within the power converter) in RCC. This MPPT method would not be feasible for converters with dc loads, three-phase loads, or probably even noisy single-phase loads; it could not be used for spacecraft or solar car applications.

Sampling and data conversion with subsequent digital division of power and voltage to approximate dP/dV is used in [32] and [33]. Convergence occurs in tens of milliseconds, but a DSP or other substantial digital circuit is required. Many other DSP-based methods have similar approaches.

In [18], [34], and [35], array capacitive effects are considered. It is shown that high frequency current ripple can yield false information in the power disturbances in the presence of capacitance (particularly large, external bypass capacitors). In these papers, techniques are suggested for compensation. Reference [18] involved general application of RCC. The analysis of capacitive effects here is similar to [18], but expanded and more thoroughly justified.

II. PROBLEM CONTEXT

The topological circuit of Fig. 1 is the context in which we investigate MPPT using RCC. Therein, a PV array is connected to a boost converter that provides a stepped-up voltage to the load. A capacitance C models parasitic capacitance of the array and possibly the intentional input filter capacitance of the converter. As will be shown, C may or may not have a significant effect; therefore, it is drawn as dashed in Fig. 1. The inductor

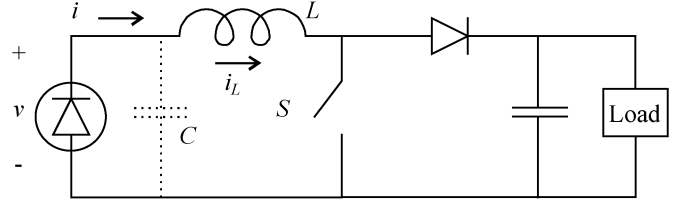


Fig. 1. PV array connected to boost circuit.

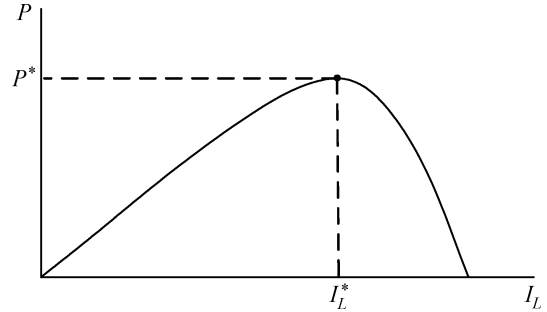


Fig. 2. Example PV array average power versus average inductor current.

current i_L , which is the same as the array current i in the absence of C , is adjusted by appropriate switching to maximize the average power output of the array. The voltage across the array is v , composed of average value V and ripple \tilde{v} . Although Fig. 1 shows a boost converter, this is not fundamental. RCC applies to any switching power converter topology.

In the boost converter case, the inductor current i_L comprises a dc component I_L and a ripple component \tilde{i}_L . At a given temperature and irradiance, i_L is adjusted and the power flow, $p = vi_L$, varies. This power is composed of average value P and ripple \tilde{p} . P varies nonlinearly in similar fashion to the curve in Fig. 2. As irradiance and temperature vary, the power curve shifts in disparate directions. As such, the MPP on the curve shifts as well. Many papers referenced above contain substantial data illustrating these points. The goal is to force I_L to track I_L^* , which is the current corresponding to the MPP, as quickly as possible, irrespective of temperature, irradiance, or other variances.

III. RIPPLE CORRELATION CONTROL

We can correlate the inductor current i_L and array power p in order to determine whether I_L is above or below I_L^* . Consider first the behavior of changes in current and power. For the moment, take $i = i_L$, which means $C = 0$. From inspection of Fig. 2, when I_L is below I_L^* , a current ripple imposed along the curve leads to an in-phase power ripple; this implies that the product of the time derivative of i_L (di_L/dt) and the time derivative of p (dp/dt) is positive. When I_L is above I_L^* , the current ripple and power ripple are out of phase, and the product of di_L/dt and dp/dt is negative. These observations can be combined as

$$\begin{aligned} \frac{di_L}{dt} \frac{dp}{dt} > 0 &\Rightarrow I_L < I_L^* \\ \frac{di_L}{dt} \frac{dp}{dt} < 0 &\Rightarrow I_L > I_L^* \end{aligned} \quad (1)$$

which will lead to one form of the RCC law.

If I_L increases when the product (1) is greater than zero, and decreases otherwise, then I_L should approach I_L^* . One way to do this is by integrating the product, such as

$$d = k \int \frac{dp}{dt} \frac{di_L}{dt} dt \quad (2)$$

where d is the duty cycle on the switch S and k is a constant, positive gain. The inductor current increases and decreases as the duty cycle d , so adjusting d should provide the correct movement of I_L . The condition $C \neq 0$ is discussed later.

Form (2) uses derivatives of signals that can be measured directly. Though differentiation of signals can be troublesome in power conversion circuits, Section IV shows how it can be handled satisfactorily.

Another way of proposing (2) involves a different approach. The optimal set point occurs when $dp/di_L = 0$; thus, the control law

$$d = \int \frac{dp}{di_L} dt \quad (3)$$

might be expected to work since the integrand would approach zero as I_L approaches I_L^* . The integrand of (3) is not generally a signal that is available in a real circuit. Prior methods discussed in the introduction relied on averaging and digital division (i.e. approximation of the derivative), or were not experimentally verified. It is difficult to achieve sufficient signal-to-noise ratio for (3) unless the convergence is made very slow.

Scaling the integrand of (3) by a positive number will change the speed and trajectory of convergence, but (3) would still converge. Consider an alternate control law, with scaling of the integrand by $(di_L/dt)^2$, which is positive so long as i_L is changing

$$d = k \int \frac{dp}{di_L} \left(\frac{di_L}{dt} \right)^2 dt = k \int \frac{dp}{dt} \frac{di_L}{dt} dt. \quad (4)$$

This yields the same law as (2), but determined from an alternative viewpoint. This integral law will drive dp/di_L to zero. Equations (1)–(4) also apply if voltage is substituted for current; however, a negative value for k would be used instead, since current and voltage are inversely related in a PV array.

A full theoretical proof of convergence of general RCC was shown in [19] and [21]. The conditions under which the control converges asymptotically to the optimum are 1) that P is unimodal and 2) that the current derivative is zero only for a finite number of time instants in a cycle. The former condition is met by PV arrays and the latter if regular switching occurs and the boost converter is in continuous conduction mode.

The asymptotic convergence is a distinguishing feature of RCC compared to traditional P&O. In the latter methods, one never really knows if the average value is at the optimum or not, and if so, one is guaranteed not to stay at the optimum. Another distinguishing feature is that convergence speed is on the order of the switching frequency. An advantage is that the perturbation is caused by the innate switching of the converter. That is, no artificial (external) disturbance needs to be added. RCC can be thought of as P&O, with the perturbation inherent and the observation as an integrator that drives the error to zero. Though

ripple is often treated as undesirable and should be eliminated if possible, no practical amount of filtering can eliminate it entirely. RCC uses whatever ripple is already present.

IV. DERIVATIVE TERMS

The differentiated signals of (2) would normally be considered a problem in practical circuit design. There are several straightforward techniques to address this complication. See [18] and [21] for a lengthier discussion.

A. High-Pass Filters

The derivatives can be approximated with high-pass filters instead of true derivatives. The cutoff frequency of the filter is set to be higher than the ripple frequency. This reduces high frequency noise problems. In [18], [21], it is proven that high-pass filtering does not affect the convergence of the RCC. It is important that the high-pass filters have the same cutoff frequency, otherwise slightly different phase shift for power and voltage or current would result.

B. Ripple Components

Ripple components can be used directly in place of derivatives. It can be shown [19], [21] that a sufficient condition of convergence is that the derivatives of power and current have a 90° phase shift. This makes intuitive sense because the product of sine waves with 90° phase separation has zero average, in which case the integral of the product ripples about a constant value. The control law becomes

$$d = k \int \tilde{i}_L \tilde{p} dt. \quad (5)$$

Here, the ripple is obtained by high-pass filtering. Compared to Section IV-A, however, the cutoff frequency is well below the switching frequency. This is desirable in a low-noise sense, but slows the dynamics and delays the convergence.

C. Derivatives Already Present

The derivative of the inductor current is approximately the scaled voltage across the inductor (ideally they are identical). Thus, by sensing the inductor voltage, which is normally easier than sensing the inductor current, we obtain the derivative information scaled by a factor $1/L$. The nonidealities in the inductor (resistance, core loss) have a small effect since the time constant of the inductor is much larger than the switching period in a practical converter.

V. ALTERNATIVE CONTROL LAWS

Sign information about the derivatives can be used instead of derivative information in RCC, as per the discussion beginning Section III. For example, one useful control law is

$$d = k \int \text{sign} \left(\frac{di_L}{dt} \right) \text{sign} \left(\frac{dp}{dt} \right) dt. \quad (6)$$

In this scenario, the noise caused by differentiation is clipped by the sign function. This is easily done in electronics hardware using simple logic or by saturating op-amp circuits, or can be

implemented with inexpensive synchronous demodulator integrated circuits (ICs).

This method has also been mathematically proven to work [21]. In the context of motor drives [36], this method was shown (in simulation) to have a convenient bounding effect that can make choosing k straightforward. It is also a convenient basis for hysteresis RCC [21], [23], [24]. The sign functions in the integrand are advantageous from a noise standpoint, though the integrand never asymptotically approaches zero. Another alternative is to bind the integrand instead, such that law (2) is preserved if the derivatives are small. Similarly, (6) can be applied to (5), albeit with slower dynamics due to the low filter cutoff frequency.

In some cases the sign information relates directly to the gating signals. For example, in the Fig. 1 system, the switching state q of switch S is 0 or 1 for off or on, respectively. The sign of the current derivative, neglecting nonidealities of the inductor, is approximately $(2q-1)$. A gating signal proportional to q is readily available in most real circuits.

VI. ARRAY OUTPUT CAPACITANCE

A PV array has stray capacitance that can be modeled as a capacitor across its output terminals. In addition, it is common to place a large capacitor at the input to the boost converter, particularly if there is a long wire connection between the array and the converter. This capacitance causes phase shift of current and power ripple that adversely affects convergence of the RCC. In other words, a capacitor makes $i \neq i_L$.

Take the array to be modeled as a nonlinear voltage source, $v = f(i)$, with a parallel capacitance C as shown in Fig. 1. The dc value of i is I and the ripple component is \tilde{i} . The current \tilde{i} differs from \tilde{i}_L due to the capacitance, though I and I_L are same in the steady state. The potential, practical problem is that the circuit designer only has access to i_L or \tilde{i}_L . Thus, the stray and intentional capacitances are effectively lumped together.

To see the implications, consider the linearized power out of the capacitor into the boost converter. This power is

$$p = f(i)i_L \quad (7)$$

which is the actual, measurable power available for an RCC law. The power $f(i)i$ on the left side of C in Fig. 1 is generally not measurable, though it gives the true correlation.

The steady-state, optimal set point is given by solving

$$\left. \frac{dp}{di} \right|_{i=I_L} = 0 = -R_0 I_L + f(I_L) \quad (8)$$

for I_L , where $R_0 = -(df/di)|_{i=I_L}$.

Linearizing (7) about an operating point I_L , converting to Laplace variables, and making appropriate substitutions yields

$$\frac{\tilde{p}}{\tilde{i}_L} = \frac{-R_0 I_L + f(I_L) + s\tau_0 f(I_L)}{1 + s\tau_0} \quad (9)$$

where $\tau_0 = R_0 C$.

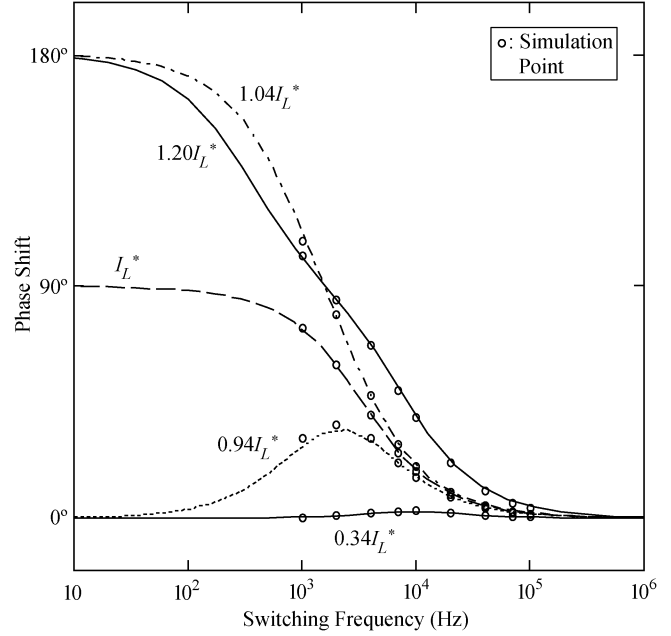


Fig. 3. Phase shift of power ripple with respect to current ripple for different current operation points; PV array model with $10 \mu\text{F}$ external capacitor.

In the limit as s goes to zero (the perturbation frequency approaches dc)

$$\left. \frac{\tilde{p}}{\tilde{i}_L} \right|_{s \rightarrow 0} = -R_0 I_L + f(I_L) \quad (10)$$

which mirrors (8). That is, at low perturbation frequencies, the disturbance in inductor current versus the disturbance in array power produces dp/di as we desire. At higher frequencies, the characteristic breaks down. In the high-frequency limit

$$\left. \frac{\tilde{p}}{\tilde{i}_L} \right|_{s \rightarrow \infty} = f(I_L) \quad (11)$$

which has a phase shift of zero. Thus for high frequencies the RCC law cannot distinguish between operating points. For proper function of the RCC, the phase shift should be 90° at I_L^* and 0° or $\pm 180^\circ$ below and above I_L^* , respectively. Thus, without compensation, there is a practical limit on switching frequency in RCC in cases where array capacitance is present. Fig. 3 shows the theoretical (curves) and simulated (points) phase response for several set points using a PV array model (given in [37] and parameters set to match the characteristics of the PV array used later in Section IX) with $10 \mu\text{F}$ of capacitance. Note the good agreement between results obtained from the small-signal model derived in (9) and those from simulation. Notice that all operating points ultimately approach zero degree phase shift. Ideally, below I_L^* , only a 0° phase shift would occur at all frequencies. Above I_L^* , a 180° shift would occur. In Fig. 3, for example, a switching frequency of 2 kHz or more yields suboptimal results.

At lower frequencies (< 1 kHz), the response is satisfactory. At high frequencies, it is apparent that the gradient information

is lost. Current-based control can only be used at low frequencies, unless a suitable estimator for i can be developed. For example, a single-pole low-pass filter applied to i_L can extend the frequency range greatly, especially if the array time constant can be approximated accurately. However, this requires some knowledge of the array and its capacitance. This is generally a disadvantage and not an easy task since the junction capacitance of a solar cell varies considerably with temperature and operating point.

VII. MITIGATING ARRAY CAPACITANCE USING VOLTAGE CORRELATION

One straightforward method of eliminating the phase shift caused by C is to correlate array power with voltage, instead of inductor current. That is

$$d = k \int \frac{dp}{dt} \frac{dv}{dt} dt = k \int \frac{dp}{dv} \left(\frac{dv}{dt} \right)^2 dt. \quad (12)$$

In the low frequency condition, (12) will produce the same operating point as (2) since dp/dv is zero, just as dp/di_L . Since voltage and current are inversely related in a PV array, k should be a negative constant in this case.

From a phase shift perspective, consider the correlation of voltage ripple and power ripple with linearization, just as for current ripple and power ripple in the previous section. For this analysis, it is convenient to define the internal cell current as $i = g(v)$ and $p = vi_L$. Here, the dc voltage V is adjusted instead of I_L , but the results are equivalent since $g^{-1} = f$. That is, there is a unique $I_L^* = g(V^*)$.

Linearization of p with appropriate substitutions yields the transfer function

$$\frac{\tilde{p}}{\tilde{v}} = g(V) + V \left. \frac{dg}{dv} \right|_{v=V} - sCV. \quad (13)$$

The first two terms on the RHS are wanted. They sum to zero at $V = V^*$. At low frequencies

$$\left. \frac{\tilde{p}}{\tilde{v}} \right|_{s \rightarrow 0} = g(V) + V \left. \frac{dg}{dv} \right|_{v=V} \quad (14)$$

as required. At high frequencies, the wanted terms of (13) vanish. The phase shift approaches -90° for all (positive) values of V .

Recall that a negative value for k is used, so in one sense the RCC performs correctly. That is, when V is optimal, we have the 90° phase shift as we desire. However, at high frequencies the phase shift is almost 90° for other values of V , which means it will be hard to distinguish among operating points and convergence will be slow.

Fig. 4 shows a theoretical (curves) and simulated (points) phase response of (13) for various set points. Note the good correlation between the small-signal model in (13) and simulation. Observe that the correct behavior is obtained for switching frequencies up to 10 kHz (90° shift only at the optimum), but at high frequencies all operating points converge. The gradient information is retained, but becomes harder to distinguish. Small

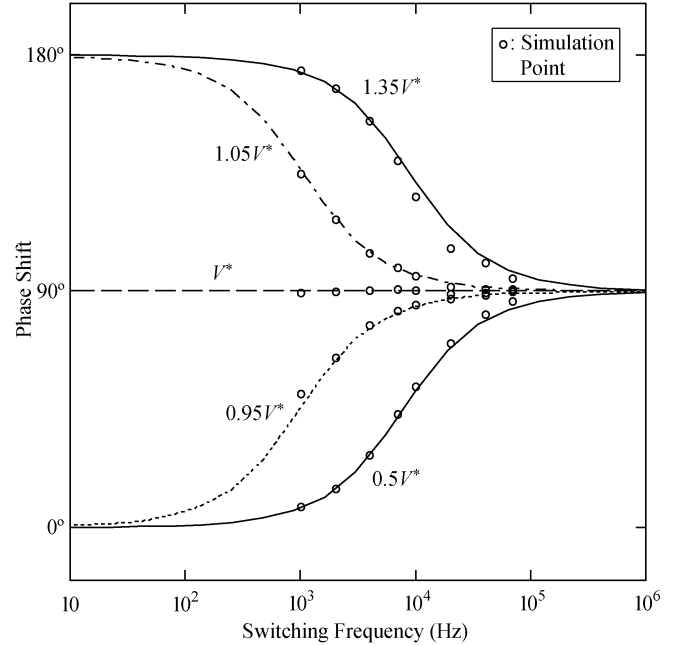


Fig. 4. Phase shift of power ripple with respect to voltage ripple for different voltage operation points; PV array model with a $10 \mu\text{F}$ external capacitor.

phase shifts in the ripple signals, such as due to mismatch in differentiators, will lead to less optimal behavior. Thus, there is a practical limit on switching frequency.

Voltage-based RCC requires no estimator for proper high frequency convergence as current-based control does. It requires no parameter knowledge of the array. Generally, it should be easier to implement than the current-based method under normal circumstances and is preferred for the simulation and experimental studies that follow.

VIII. IMPLEMENTATION

One possible circuit implementation for RCC is shown in Fig. 5. It is directly based on the RCC law (12). High-pass filters are used for differentiators. Analog multipliers are used to compute power and the product for the integrand of (12). Current is sensed by a small resistance in series with the PV panel.

Alternative implementations are possible, depending on the form used to approximate the differentiator. However, the method shown only uses five op-amps, two multipliers, and a few readily available resistors and capacitors. The ICs come in various packages that would reduce part count. The low-quantity, retail cost of the circuit of Fig. 5 is under \$10.00 USD. This is less expensive than most DSP circuits including all peripherals and support hardware and is far easier to layout and validate on a printed circuit board. Ease of implementation, however, varies with one's background and preferences, so some readers may prefer digital methods [38]. Fig. 5 comprises only the control loop—sensing circuits, a gate pulse generator, and the boost circuit (Fig. 1) are also required, just as in other MPPT methods.

For the same ripple magnitude requirement, a smaller inductor size can be achieved at a higher switching frequency. During steady-state operation, power loss can be reduced by decreasing ripple magnitude. This can be done by increasing the

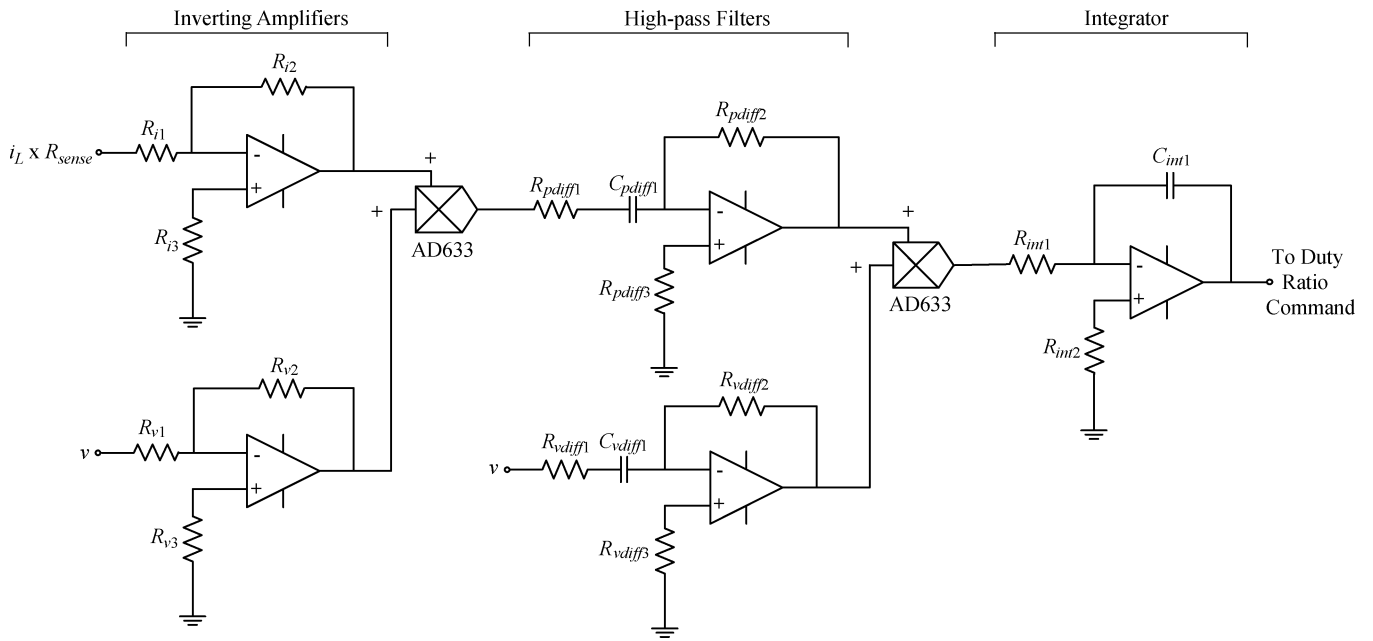


Fig. 5. Schematic of RCC circuit used in experimental studies. Several variations and simplifications are possible.

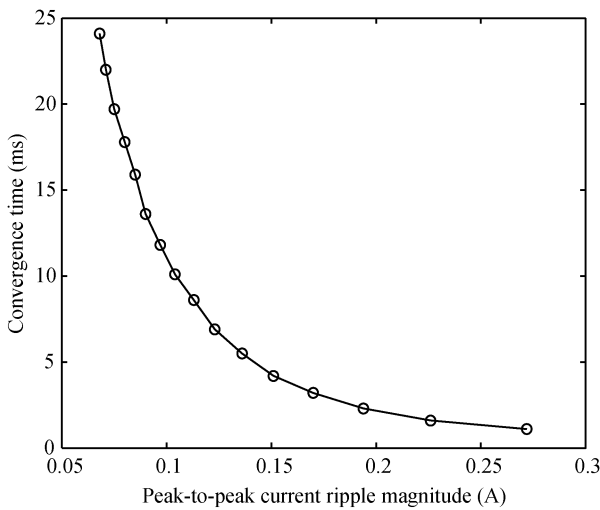


Fig. 6. Convergence time versus current ripple magnitude at fixed switching frequency and RCC gain.

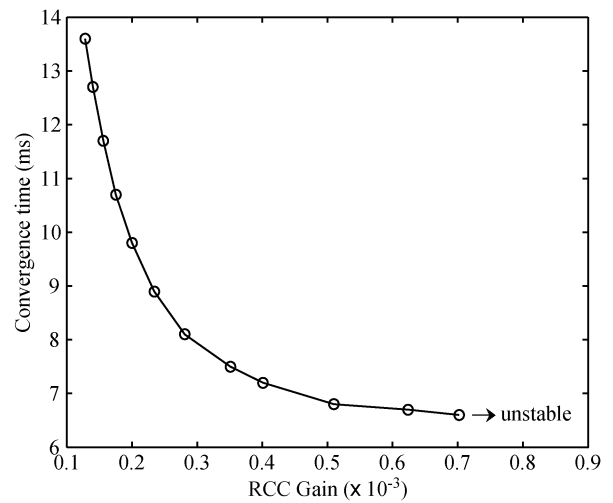


Fig. 7. Convergence time vs. RCC gain at 10 kHz and 0.09 A current ripple.

inductance L (Fig. 1). However, this increases the time constant of the system and thus the convergence time to the MPP during changes in atmospheric conditions. A boost converter (Fig. 1), with the RCC circuit (Fig. 5), was simulated for a step change in irradiance from 0.9 to 1 kW/m² and the convergence time was recorded for different current ripple magnitudes (inductor sizes), while fixing the switching frequency at 10 kHz and the RCC gain at 0.128×10^{-3} . Fig. 6 shows that convergence time decreases exponentially with increase in current ripple magnitude (or decrease in inductor size).

On the other hand, if the current ripple magnitude and switching frequency are kept constant, the convergence time can be decreased by increasing the RCC gain. Fig. 7 shows how the convergence time decreases exponentially with increase in

gain for a current ripple of 0.09 A. However, no appreciable improvement in convergence time is obtained at higher gains and the system becomes unstable when the gain is too high. The same behavior can be noticed for different current ripple magnitudes.

Therefore, wanted convergence times can be attained by trading off inductor size and RCC gain, as long as the system remains stable. However, there are other factors that also affect the choice of inductor size. For example, the resistive power loss due to a bigger inductor might outweigh the decrease in power loss due to smaller current ripple. Noise is always present on measured signals and good signal-to-noise ratio is important for the proper functioning of RCC. Aggressive filtering, which leads to small ripple, low signal-to-noise ratio, and more resistive power losses, is thus undesirable.

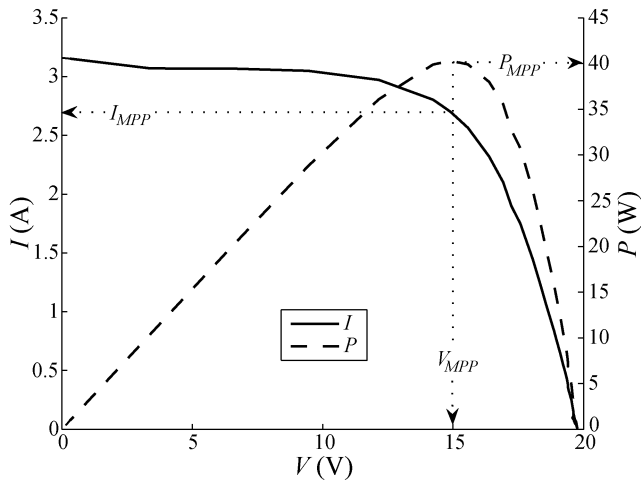


Fig. 8. Characteristic curves of S-5136 PV array (facing the sun).

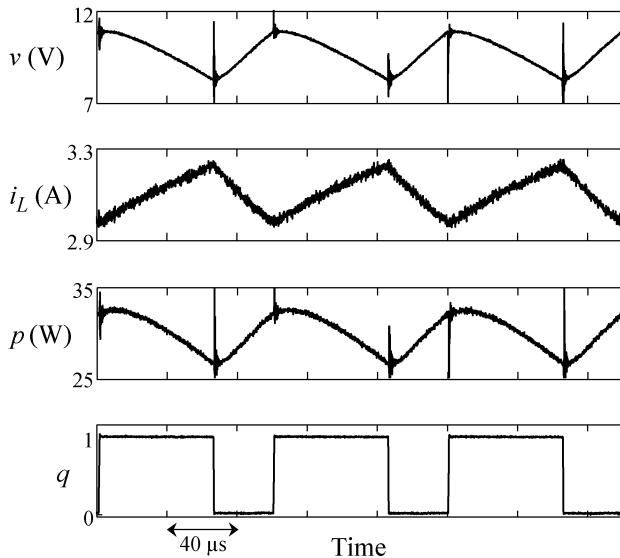


Fig. 9. Measured voltage, current, power, and gating signal for a current set point of $I_L > I_L^*$.

IX. EXPERIMENTAL STUDIES

The validity of the control method is demonstrated on a small test system. An S-5136 PV array (33 cm \times 130 cm) from Solec International Incorporation was used in this experiment. Mounted on a frame, the panel could be rotated to point directly at or away from the sun. Thus, the irradiance level on the surface of the array could be easily varied. Fig. 8 shows the measured I - V and P - V curves of the array, when directed towards the sun on a clear sunny mid-November day, in Champaign, IL. The MPP was about 40 W, occurring at about 15 V and 2.7 A. The switching frequency of the boost converter was set to 10 kHz.

To illustrate the phase shifts above and below I_L^* (Fig. 2), the voltage v , current i_L , power p , and gating signal q were captured for two different power levels. The PV array was directed towards the sun and the MPP was determined to be 36.91 W at that point of the day. In Fig. 9, a current setting of $I_L > I_L^*$ was used. The measured power was 30.34 W. The current ripple is out of phase with the power ripple and the voltage ripple is in phase with the power ripple.

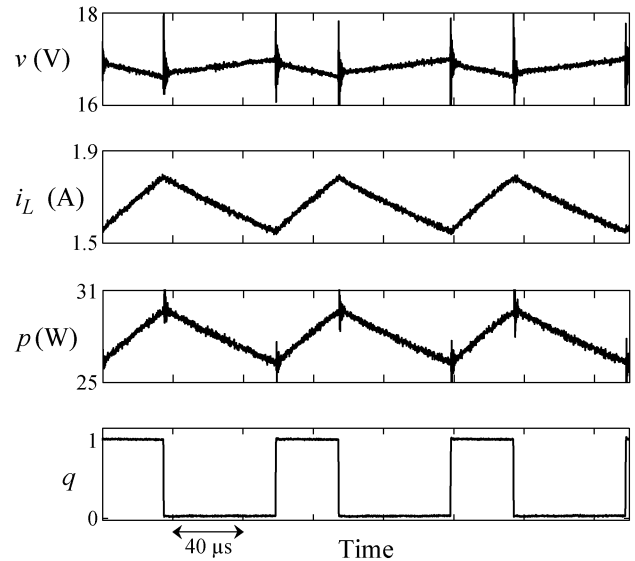


Fig. 10. Measured voltage, current, power, and gating signal for a current set point of $I_L < I_L^*$.

TABLE I
OPEN-LOOP VERSUS CLOSED-LOOP POWER MEASUREMENTS

Open-loop Power (W)	Closed-loop Power (W)	% Error
16.35	15.37	5.99
18.90	17.88	5.40
21.11	19.91	5.68
22.76	21.56	5.27
25.03	23.90	4.51
26.87	25.70	4.35
29.64	28.61	3.48
31.11	30.22	2.86
33.00	32.07	2.82
35.07	34.06	2.88
37.17	35.87	3.50
37.92	36.52	3.69

In Fig. 10, the set point was such that $I_L < I_L^*$ and the measured power was 28.02 W. The current ripple is clearly in phase with the power ripple, while voltage ripple is out of phase with the power ripple. These two figures confirm the desired phase relationship between ripple in power and current or voltage. The significant point is that the frequency is 10 kHz and the perturbation is natural—not due to an artificial injected disturbance.

To determine how well the RCC circuit tracks the MPP of the PV array, the duty cycle was first varied manually (open-loop) until the maximum average power output was recorded. Then the RCC loop was closed and the power was measured again. This was repeated with the PV array oriented at different angles to the sun, thus varying the irradiance level on the surface of the array. Table I contains open-loop and closed-loop data for twelve different cases. Notice that there is about 1 W difference between the open-loop and closed-loop powers. This difference seems to be consistent for all the cases, even though the percentage error increases as the power decreases. Note that fluctuations in atmospheric conditions between the two sets of measurements also affect the error. The smaller error reported in [17] can be explained by the difference in implementation.

A better understanding of this discrepancy can be obtained by looking at the open-loop and closed-loop power waveforms

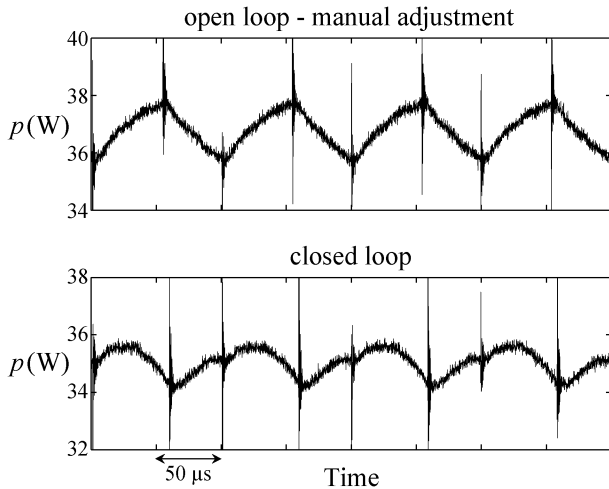


Fig. 11. Measured power waveforms for open-loop and closed-loop cases.

in Fig. 11—the measured average power was 36.97 W and 35.42 W, respectively. The shape of the closed-loop power waveform clearly shows that the operating point is oscillating about or near the MPP (Fig. 2). However, the shape of the open-loop power waveform implies that the true maximum power does not occur at the commonly depicted MPP. This condition was investigated in [36]. The characteristic power curve (Fig. 2) of a PV array is a static curve based on dc voltage and current; ripple components have not been considered. Based on [36], the control law

$$d = k \int \frac{dp}{dv} dt \quad (15)$$

should converge to the true MPP, but the integrand is a signal that is not readily available in a circuit. The RCC law (12) used in this experiment has a weighting factor of $(dv/dt)^2$, which brings the convergence closer to the MPP of the static curve. This also explains the consistent discrepancy observed in the experiment. According to [36], a control law

$$d = k \int \frac{dp}{dt} \text{sign} \left(\frac{dv}{dt} \right) dt \quad (16)$$

would converge to a point closer to the true MPP; the weighting factor is only $\text{abs}(dv/dt)$ in this case. Decreasing the voltage (and current) ripple magnitude, which affect the weighting factor, should lead to convergence even closer to the true MPP.

A transient of control start-up is shown in Fig. 12. Initially, the circuit is in open-loop mode with a given duty cycle. The RCC circuit is switched on and subsequently, as can be seen from Fig. 12, the duty cycle command d and power converge close to the MPP in about 20 ms. Upon activation, there is a distinct drop in duty cycle—this is due to how the control changeover is implemented and not anything fundamentally associated with RCC.

As shown in Section VIII, convergence speed can be increased, if necessary, by using more controller gain. When doing so, a larger inductor would be necessary to reduce the voltage and power ripple. If the ripple and gain are too high,

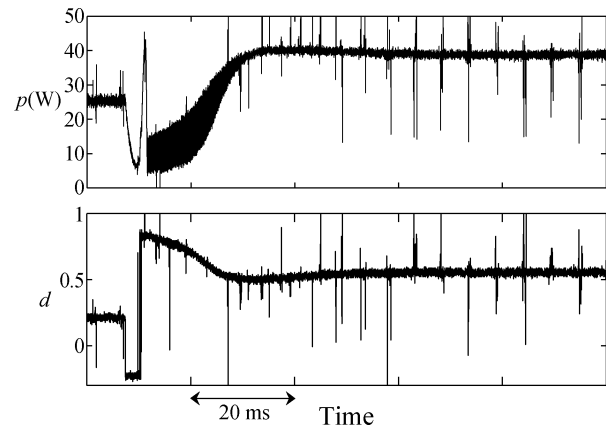


Fig. 12. Measured power (top) and duty cycle command (bottom) transient upon control activation.

the control can saturate and exhibit limit cycle behavior. Use of alternative versions of the control law can decouple the ripple from the gain choice. This was discussed in [39] in the context of electric machines.

With the single PV array used in this experiment, no occurrence of multiple local maxima due to partial shading was noted; when partially shaded, the current coming out the array was found to be zero. If multiple arrays connected in series and/or parallel, which could result in multiple local maxima, were to be used, RCC might not track the true MPP since it only drives dP/dI or dP/dV to zero. In this case, the solution might be a two-stage approach as in [40] and [41]. In the first stage, the unwanted local maxima are bypassed to bring operation close to the true MPP and in the second stage, RCC can be used to track it. However, RCC is better suited for modular systems, where each PV array is connected to its own MPP tracker unit—then multiple local maxima should not be an issue.

X. CONCLUSION

A method for MPPT of photovoltaic arrays was set forth and shown to work in hardware. The method is distinguished by very rapid response time and steady-state convergence close to the true optimum using as input only the naturally occurring ripple inherent to the power converter system. Effects of array capacitance were discussed. A straightforward, low-cost, analog circuit was shown as an example of implementation.

ACKNOWLEDGMENT

The authors would like to thank R. Turnbull, R. Reppa, and D. Logue for their early contributions and discussions involving this work.

REFERENCES

- [1] P. D. Van den Heever, S. Oberholzer, and J. H. R. Enslin, "High-efficient solar panel/wind turbine converter with maximal power control," in *Proc. Eur. Conf. Power Electron. Appl.*, 1989, pp. 663–668.
- [2] J. J. Schoeman and J. D. van Wyk, "A simplified maximal power controller for terrestrial photovoltaic panel arrays," in *Proc. 13th Annu. IEEE Power Electron. Spec. Conf.*, 1982, pp. 361–367.
- [3] C. R. Sullivan and M. J. Powers, "A high-efficiency maximum power point tracker for photovoltaic arrays in a solar-powered race vehicle," in *Proc. 24th Annu. IEEE Power Electron. Spec. Conf.*, 1993, pp. 574–580.

- [4] A. F. Boehringer, "Self-adapting dc converter for solar spacecraft power supply," *IEEE Trans. Aerosp. Electron. Syst.*, vol. AES-4, no. 1, pp. 102–111, Jan. 1968.
- [5] E. E. Landsman, *Maximum Power Point Tracker for Solar Arrays*. Boston, MA: Mass. Inst. Technol. Lincoln Labs, 1978.
- [6] S. Yuvarajan and S. Xu, "Photo-voltaic power converter with a simple maximum-power-point-tracker," in *Proc. Int. Symp. Circuits Syst.*, 2003, pp. III-399–III-402.
- [7] M. A. El-Shibini and H. H. Rakha, "Maximum power point tracking technique," in *Proc. Integr. Res., Ind. Educ. Energy Commun. Eng. Electrotech. Conf.*, 1989, pp. 21–24.
- [8] C.-T. Pan, J.-Y. Chen, C.-P. Chu, and Y.-S. Huang, "A fast maximum power point tracker for photovoltaic power systems," in *Proc. 25th Annu. Conf. IEEE Ind. Electron. Soc.*, 1999, pp. 390–393.
- [9] G.-J. Yu, M.-W. Jung, J. Song, I.-S. Cha, and I.-H. Hwang, "Maximum power point tracking with temperature compensation of photovoltaic for air conditioning system with fuzzy controller," in *Proc. 25th IEEE Photovolt. Spec. Conf.*, 1996, pp. 1429–1432.
- [10] K. Ro and S. Rahman, "Two-loop controller for maximizing performance of a grid-connected photovoltaic-fuel cell hybrid power plant," *IEEE Trans. Energy Conv.*, vol. EC-13, no. 3, pp. 276–281, Sep. 1998.
- [11] T. Kitano, M. Matsui, and D.-H. Xu, "Power sensor-less MPPT control scheme utilizing power balance at DC link-system design to ensure stability and response," in *Proc. 27th Annu. Conf. IEEE Ind. Electron. Soc.*, 2001, pp. 1309–1314.
- [12] G. W. Hart, H. M. Branz, and C. H. Cox, "Experimental tests of open-loop maximum-power-point tracking techniques for photovoltaic arrays," *Solar Cells*, vol. 13, pp. 185–195, Dec. 1984.
- [13] F. Huang, G. Zhimin, T. Forughian, and D. Tien, "A new microcontroller based solar energy conversion modular unit," in *Proc. Power Conv. Conf.*, 1997, pp. 697–700.
- [14] M. Matsui, T. Kitano, and D. Xu, "A simple maximum photovoltaic power tracking technique utilizing system inherent limit cycle phenomena," in *Proc. 38th Annu. Ind. Appl. Conf.*, 2003, pp. 2041–2047.
- [15] T. ESRAM and P. L. Chapman, "Comparison of photovoltaic array maximum power point tracking techniques," *IEEE Trans. Energy Conv.*, to be published.
- [16] P. T. Krein, "Ripple correlation control, with some applications," in *Proc. 1999 IEEE Int. Symp. Circuits Syst.*, 1999, pp. 283–286.
- [17] P. Midya, P. T. Krein, R. J. Turnbull, R. Reppa, and J. Kimball, "Dynamic maximum power point tracker for photovoltaic applications," in *Proc. 27th Annu. IEEE Power Electron. Spec. Conf.*, 1996, pp. 1710–1716.
- [18] D. L. Logue and P. T. Krein, "Observer-based techniques in ripple correlation control applied to power electronic systems," in *Proc. 32nd Annu. IEEE Power Electron. Spec. Conf.*, 2001, pp. 2014–2018.
- [19] —, "Optimization of power electronic systems using ripple correlation control: a dynamic programming approach," in *Proc. 32nd Annu. IEEE Power Electron. Spec. Conf.*, 2001, pp. 459–464.
- [20] C. C. Hang and K. K. Sin, "On-line auto tuning of PID controllers based on cross-correlations technique," *IEEE Trans. Ind. Electron.*, vol. 38, no. 6, pp. 428–437, Dec. 1991.
- [21] D. L. Logue, "Power Electronic Building Block Applications in Optimization, Control, and Simulation," Ph.D. dissertation, Univ. Illinois Urbana-Champaign, Urbana, 2000.
- [22] V. Arcidiacono, S. Corsi, and L. Lambri, "Maximum power point tracker for photovoltaic plants," in *Proc. IEEE Photovolt. Spec. Conf.*, 1982, pp. 507–512.
- [23] Y. H. Lim and D. C. Hamill, "Simple maximum power point tracker for photovoltaic arrays," *Electron. Lett.*, vol. 36, pp. 997–999, May 2000.
- [24] —, "Synthesis, simulation and experimental verification of a maximum power point tracker from nonlinear dynamics," in *Proc. 32nd Annu. IEEE Power Electron. Spec. Conf.*, 2001, pp. 199–204.
- [25] H. Sugimoto and H. Dong, "A new scheme for maximum photovoltaic power tracking control," in *Proc. Power Conv. Conf.*, 1997, pp. 691–696.
- [26] A. Al-Amoudi and L. Zhang, "Optimal control of a grid-connected PV system for maximum power point tracking and unity power factor," in *Proc. 7th Int. Conf. Power Electron. Variable Speed Drives*, 1998, pp. 80–85.
- [27] L. Stamenic, M. Greig, E. Smiley, and R. Stojanovic, "Maximum power point tracking for building integrated photovoltaic ventilation systems," in *Proc. 28th IEEE Photovolt. Spec. Conf.*, 2000, pp. 1517–1520.
- [28] K. K. Tse, M. T. Ho, H. S.-H. Chung, and S. Y. Hui, "A novel maximum power point tracker for PV panels using switching frequency modulation," *IEEE Trans. Power Electron.*, vol. 17, no. 6, pp. 980–989, Nov. 2002.
- [29] H. S.-H. Chung, K. K. Tse, S. Y. R. Hui, C. M. Mok, and M. T. Ho, "A novel maximum power point tracking technique for solar panels using a SEPIC or Cuk converter," *IEEE Trans. Power Electron.*, vol. 18, no. 3, pp. 717–724, May 2003.
- [30] A. Cocconi, S. Cuk, and R. D. Middlebrook, "High-frequency isolated 4 kW photovoltaic inverter for utility interface," *Adv. Switched-Mode Power Conv.*, vol. III, pp. 325–345, 1983.
- [31] M. Calais and H. Hinz, "A ripple-based maximum power point tracking algorithm for a single-phase, grid-connected photovoltaic system," *Solar Energy*, vol. 63, pp. 227–282, Jul. 1998.
- [32] S. J. Chiang, K. T. Chang, and C. Y. Yen, "Residential photovoltaic energy storage system," *IEEE Trans. Ind. Electron.*, vol. 45, no. 3, pp. 385–394, Jun. 1998.
- [33] J. A. M. Bleijs and A. Gow, "Fast maximum power point control of current-fed DC-DC converter for photovoltaic arrays," *Electron. Lett.*, vol. 37, pp. 5–6, Jan. 2001.
- [34] A. Brambilla, M. Gambarara, A. Garutti, and F. Ronchi, "New approach to photovoltaic arrays maximum power point tracking," in *Proc. 30th Annu. IEEE Power Electron. Spec. Conf.*, 1999, pp. 632–637.
- [35] N. Kasa, T. Iida, and H. Iwamoto, "Maximum power point tracking with capacitor identifier for photovoltaic power system," in *Proc. 8th Int. Conf. Power Electron. Variable Speed Drives*, 2000, pp. 130–135.
- [36] J. R. Wells, P. L. Chapman, and P. T. Krein, "Fundamental aspects of ripple correlation control of electric machinery," in *Proc. 34th Annu. IEEE Power Electron. Spec. Conf.*, 2003, pp. 1659–1662.
- [37] H. Yamashita, K. Tamahashi, M. Michihira, A. Tsuyoshi, K. Amako, and M. Park, "A novel simulation technique of the PV generation system using real weather conditions," in *Proc. Power Conv. Conf.*, 2002, pp. 839–844.
- [38] K. K. Tse, B. M. T. Ho, H. S.-H. Chung, and S. Y. R. Hui, "A comparative study of maximum power point trackers for photovoltaic panels using switching frequency modulation," *IEEE Trans. Ind. Electron.*, vol. 51, no. 2, pp. 410–418, Apr. 2004.
- [39] J. R. Wells, P. L. Chapman, and P. T. Krein, "Applications of ripple correlation control of electric machinery," in *Proc. IEEE Int. Elect. Machines Drives Conf.*, 2003, pp. 1498–1503.
- [40] K. Irisawa, T. Saito, I. Takano, and Y. Sawada, "Maximum power point tracking control of photovoltaic generation system under non-uniform insolation by means of monitoring cells," in *Proc. 28th IEEE Photovolt. Spec. Conf.*, 2000, pp. 1707–1710.
- [41] K. Kobayashi, I. Takano, and Y. Sawada, "A study on a two stage maximum power point tracking control of a photovoltaic system under partially shaded insolation conditions," in *Proc. IEEE Power Eng. Soc. General Meeting*, 2003, pp. 2612–2617.



Trishan ESRAM (S'00) was born in Mauritius on March 8, 1980. He received the B.S.E.E. degree from Northeastern University, Boston, MA, in 2003 and the M.S.E.E. degree from the University of Illinois at Urbana-Champaign (UIUC), in 2004 where he is currently pursuing the Ph.D. degree in electrical engineering.

He has been a Research Assistant in the Electrical and Computer Engineering Department, UIUC, since 2003. His research interests include optimal control of power converters and alternative energy sources.



Jonathan W. Kimball (M'96-SM'05) received the B.S. degree in electrical and computer engineering from Carnegie Mellon University, Pittsburgh, PA, in 1994 and the M.S. degree in electrical engineering from the University of Illinois at Urbana-Champaign (UIUC) in 1996.

He worked for Motorola, Phoenix, AZ, designing IGBT modules for industrial applications. He then joined Baldor Electric, Fort Smith, AR, where he designed industrial adjustable speed drives ranging 1–200 hp. In 2003, he returned to UIUC as a Research Engineer. He is also Vice President of Engineering for SmartSpark Energy Systems, Inc., Champaign, IL. Research interests include motor control inverters, switched-capacitor converters, converters for alternative energy sources, and modeling and control of dc-dc converters.

Mr. Kimball is a member of Eta Kappa Nu, Tau Beta Pi, and Phi Kappa Phi.



Philip T. Krein (S'76–M'82–SM'93–F'00) received the B.S. degree in electrical engineering and the A.B. degree in economics and business from Lafayette College, Easton, PA, and the M.S. and Ph.D. degrees in electrical engineering from the University of Illinois, Urbana.

He was an Engineer with Tektronix, Beaverton, OR, then returned to the University of Illinois. At present he holds the Grainger Endowed Director's Chair in Electric Machinery and Electromechanics as Director of the Grainger Center for Electric Machinery and Electromechanics. He authored *Elements of Power Electronics* (Oxford, UK: Oxford Univ. Press, 1998). In 2001, he helped initiate the International Future Energy Challenge (a major student competition involving fuel cell power conversion and energy efficiency for machines). He holds eight U.S. patents. His research interests address all aspects of power electronics, machines, and drives, with emphasis on nonlinear control approaches.

Dr. Krein was a Senior Fulbright Scholar at the University of Surrey, Surrey, UK, from 1997 to 1998, a University Scholar in 1999 (the highest research award at the University of Illinois), and received the IEEE William E. Newell Award in Power Electronics in 2003. At present, he is Editor of *IEEE POWER ELECTRONICS LETTERS*. From 1999 to 2000, he was President of the IEEE Power Electronics Society, and from 2003 to 2004, served on the IEEE Board of Directors for Division II. He is a Registered Professional Engineer in Illinois and Oregon.



Patrick L. Chapman (S'94–M'00–SM'05) received the B.S. and M.S. degrees from the University of Missouri-Rolla, in 1996 and 1997, respectively, and the Ph.D. degree from Purdue University, West Lafayette, IN, in 2000.

Currently, he is a Grainger Associate and Assistant Professor in the Department of Electrical and Computer Engineering, University of Illinois at Urbana-Champaign, Urbana. He is a co-founder of SmartSpark Energy Systems, Inc. His research interests, within power electronics, include integrated design, automated modeling, hybrid energy systems, and energy harvesting.

Dr. Chapman received the National Science Foundation CAREER Award, the Office of Naval Research Young Investigator Award, and was named the Richard M. Bass Outstanding Young Power Electronics Engineer in 2006. He is an Associate Editor for the *IEEE TRANSACTIONS ON POWER ELECTRONICS* and a Member-at-Large for the IEEE Power Electronics Society Administrative Committee.



Pallab Midya (SM'96) received the B.Tech. degree from the Indian Institute of Technology, Kharagpur, in 1988, the M.S. degree from Syracuse University, Syracuse, NY, in 1990, and the Ph.D. degree in electrical engineering from the University of Illinois at Urbana-Champaign in 1995.

He joined Motorola Labs, Schaumburg, IL, in 1995 and then Freescale Semiconductor, Lake Zurich, IL (a spinoff of Motorola), in 2004. He is currently a Distinguished Member of the Technical Staff. He has 25 issued and ten pending U.S. patents. He has authored 25 IEEE, IEE, and AES papers. He introduced supply modulation as a method to increase RF transmitter efficiency. He was the chief architect of an IC that doubled the transmitter efficiency of Motorola's satellite phone. This technology has since been incorporated into Motorola cellular phones. He initiated a research program for direct digital RF generation and amplification to create modulated RF signal using a switching amplifier. He has been a technical lead in Motorola's Digital Switching Audio Amplifier program.

Dr. Midya received the Richard Bass Outstanding Young Power Electronics Engineer Award from IEEE and the Young Alumni Achievement Award from the University of Illinois in 2002. He is a member of Sigma Xi, the HKN Electrical Engineering Honor Society, and the Audio Engineering Society.